Journal of Integrated Coastal Zone Management / Revista de Gestão Costeira Integrada, 16(3):343-355 (2016)

Journal of Integrated Coastal Zone Management
Revista de Gestão Costeira Integrada

http://www.aprh.pt/rgci/pdf/rgci-660_Carmo.pdf | DOI: 10.5894/rgci660

Nonlinear and dispersive wave effects in coastal processes*

José Simão Antunes do Carmo [a]

ABSTRACT

Numerical models are useful instruments for studying complex superposition of wave-wave and wave-current interactions in coastal and estuarine regions, and to investigate the interaction of waves with complex bathymetries or structures built in near-shore areas. The ability of the standard Boussinesq and Serre or Green and Naghdi equations to reproduce these nonlinear processes is well known. However, these models are restricted to shallow water conditions, and addition of other terms of dispersive origin has been considered since the 90's, particularly for approximations of the Boussinesq-type. Using the general wave theory in shallow water conditions, the different approaches commonly used in hydrodynamics studies in river systems, estuaries and coastal zones are initially addressed. Then, to allow applications in a greater range of shallow waters, namely in intermediate water conditions, a new set of extended Serre equations, with additional terms of dispersive origin, is presented and tested with available data in the literature. The hydrodynamic module, composed of the extended Serre equations, is then used as part of a morphodynamic model, which incorporates two more equations taking into account various processes of sediment transport. The wave velocity-skewness and the acceleration-asymmetry are taken into account and discussed based on numerical results and physical considerations.

Keywords: Wave theory in shallow waters, extended Serre equations, sediment transport, Bailard model, wave acceleration-asymmetry, wave velocity-skewness.

RESUMO

Efeitos não-lineares e dispersivos da onda nos processos costeiros

Os modelos numéricos são instrumentos úteis para estudar a propagação de ondas em meios com diferentes características, desde águas profundas (ao largo) até condições de água pouco profunda, e investigar a interação de ondas com batimetrias complexas ou estruturas construídas em regiões costeiras e estuarinas. As capacidades de modelos do tipo Boussinesq e as equações de Serre, ou de Green e Naghdi, para reproduzir os processos não-lineares de diversas interações são bem conhecidas. No entanto, estas aproximações clássicas restringem-se a condições de águas pouco profundas. Desde meados da década de 90 têm sido desenvolvidas formulações que modificam ou acrescentam termos de origem dispersiva para aplicações mais generalizadas, particularmente em aproximações do tipo Boussinesq. Recorrendo à teoria geral das ondas em condições de águas pouco profundas, são aqui apresentadas, em primeiro lugar, as aproximações comumente usadas em estudos da hidrodinâmica em meios fluviais, estuários e zonas costeiras. Tendo como objetivo alargar o campo de aplicação a outros domínios, em particular a condições de águas intermédias, é em seguida apresentada e testada com dados experimentais uma formulação das equações clássicas de Serre com melhores características dispersivas lineares. Por fim, é proposto um modelo morfodinâmico 1DH composto por um módulo hidrodinâmico, que resolve as equações expandidas de Serre, e por duas equações que incorporam vários processos de transporte sedimentar. Em particular, são avaliados e discutidos termos de transporte induzidos pelo enviesamento (skewness) e pela assimetria da onda.

***Paravras-chave**: Teoria da onda em água pouco profunda, equações expandidas de Serre, transporte sedimentar, modelo de Bailard, enviesamento e assimetria da onda.*

[a] University of Coimbra, Department of Civil Engineering, 3030-788 Coimbra, Portugal. e-mail: jsacarmo@dec.uc.pt

* *Submission: 14 DEC 2015; Peer review: 2 FEB 2016; Revised: 31 MAR 2016; Accepted: 14 APR 2015; Available on-line: 9 MAY 2016*

This article contains supporting information online at http://www.aprh.pt/rgci/pdf/rgci-660_Carmo_Supporting-Information.pdf

1. Introduction

Knowledge of the flow characteristics associated with surface waves and currents, and their dependency on the bathymetry and coastal geometry, is of considerable importance when designing structures commonly found in the coastal environment, like groynes and breakwaters. Such knowledge also helps to predict the modifications thereby introduced into sea disturbance and into transport and deposition of sediments.

By the end of the 70's linear models were used to simulate the refraction effect produced by depth variation along the direction of the wave crest propagation, and the diffraction effect produced by the gradient of the wave amplitude along its crest. In the 80's other models, that take into account not only de refraction but also the diffraction process, have been proposed and commonly used by Berkhoff *et al*. (1982), Kirby & Dalrymple (1983), Booij (1983), Kirby (1984) and Dalrymple (1988), among many others. However, as they are based on the linear theory, those models should not be utilized in shallow water conditions.

Even at that time, models based on the Saint-Venant equations were frequently used in practical applications. However, as has been widely demonstrated, in shallow water conditions and for some types of waves, models based on a non-dispersive theory, of which the Saint-Venant model is an example, are limited and are not usually able to compute satisfactory results over long periods of analysis (Santos, 1985). Nowadays, it is generally accepted that for practical applications the combined gravity wave effects in shallow water conditions must be taken into account. In addition, the refraction and diffraction processes, the swelling, reflection and breaking waves, all have to be considered.

A number of factors has made it possible to employ increasingly complex mathematical models. Not only our theoretical knowledge of the phenomena involved has improved greatly, but also the numerical methods have been used more efficiently. The great advances made in computer technology, especially since the 1980s, improving information processing and enabling large amounts of data to be stored have made possible the use of mathematical models of greater complexity and with fewer restrictions.

Therefore, only models of order σ^2 ($\sigma = h_0/\lambda$), where h_0 and λ represent, respectively, depth and wavelength characteristics) or greater, of the Boussinesq or Serre types (Boussinesq, 1872; Serre, 1953), are able to reproduce several phenomena in addition to the dispersive effects, including the non-linearities resulting from wave-wave and wave-current interactions, and the waves resulting from sudden time-bed-level changes that cause tsunamis, wherein submerged landslides in reservoirs, or landslides on reservoir banks, are examples of such changes.

In the past few years, the possibility of using more powerful computational facilities along with the technological evolution and sophistication of control systems have required a thorough theoretical and experimental research designed to improve the knowledge of coastal hydrodynamics. Numerical methods aimed to applications in engineering fields more sophisticated and with a higher degree of complexity have also been developed.

In Section 2, the general shallow water wave theory is used to develop different mathematical approaches, which are nowadays the basis of the most sophisticated models in hydrodynamics and sedimentary dynamics. An extension of the Serre equations for applications in intermediate water conditions and comparisons of numerical results with physical data available in the literature are presented in Sections 3 and 4. Then, a morphodynamic model composed of this hydrodynamic module and a sediment transport model is proposed and discussed in Section 5. The sediment transport model consists on a sediment conservation equation and a dynamic equation. An improved version of Bailard model, incorporating various sediment transport processes, is used as the dynamic equation of the solid-phase model. It is shown that both the skewness and the wave asymmetry lead to an increase of the sediment transport in the wave direction.

2. Mathematical formulations

We start from the fundamental equations of the Fluid Mechanics, written in Euler's variables, relating to a three-dimensional and *quasi*-irrotational flow of a perfect fluid [Euler equations, or Navier-Stokes equations with the assumptions of non-compressibility ($d\rho/dt = div\ \vec{v} = 0$), irrotationality (rot $\vec{v} = 0$) and perfect fluid (dynamic viscosity $\mu = 0$)]:

$$\begin{aligned} &u_x + v_y + w_z = 0 \\ &u_t + uu_x + vu_y + wu_z = -p_x/\rho \\ &v_t + uv_x + vv_y + wv_z = -p_y/\rho \\ &w_t + uw_x + vw_y + ww_z = -p_z/\rho - g \\ &u_z = w_x;\ v_z = w_y;\ v_x = u_y \end{aligned} \qquad (1)$$

with $p = 0$ at $z = \eta(x,y,t)$, $w = \eta_t + u\eta_x + v\eta_y$ at $z = \eta(x,y,t)$, and $w = \xi_t + u\xi_x + v\xi_y$ at $z = -h_0 + \xi(x,y,t)$.

In these equations ρ is density, t is time, g is gravitational acceleration, p is pressure, η is free surface elevation, ξ is bottom, and (u, v, w) are velocity components.

Defining the dimensionless quantities $\varepsilon = a/h_0$ and $\sigma = h_0/\lambda$, in which a is a characteristic wave amplitude, h_0 represents water depth, and λ is a characteristic wavelength, we proceed with suitable non-dimensional variables:

$$x' = x/\lambda\ ,\ y' = y/\lambda\ ,\ z' = z/h_0\ ,\ \eta' = \eta/a\ ,$$
$$\xi' = \xi/h_0\ ,\ t' = t\sqrt{gh_0}\,/\lambda = tc_0/\lambda\ ,\ p' = p/(\rho g h_0),$$
$$u' = u/\left(a\sqrt{g/h_0}\right) = uh_0/(ac_0),$$
$$v' = v/\left(a\sqrt{g/h_0}\right) = vh_0/(ac_0),$$
$$w' = w\lambda/\left(ah_0\sqrt{g/h_0}\right) = v\lambda/(ac_0),$$

where c_0 represents critical celerity, given by $c_0 = (gh_0)^{1/2}$, η is free surface elevation, ξ represents bathymetry, u, v and w are velocity components, and p is pressure.

In dimensionless variables, without the line on the variables, the fundamental equations and the boundary conditions are written (Carmo & Seabra-Santos, 1996):

A – Fundamental equations

$$\begin{aligned}
&\text{a)}\quad u_x + v_y + w_z = 0\\
&\text{b)}\quad \varepsilon u_t + \varepsilon^2 uu_x + \varepsilon^2 vu_y + \varepsilon^2 wu_z = -p_x\\
&\text{c)}\quad \varepsilon v_t + \varepsilon^2 uv_x + \varepsilon^2 vv_y + \varepsilon^2 wv_z = -p_y\\
&\text{d)}\quad \varepsilon\sigma^2 w_t + \varepsilon^2\sigma^2 uw_x + \varepsilon^2\sigma^2 vw_y + \varepsilon^2\sigma^2 ww_z = -p_z - 1\\
&\text{e)}\quad u_z = \sigma^2 w_x\ ;\ v_z = \sigma^2 w_y\ ;\ v_x = u_y
\end{aligned} \tag{2}$$

B – Boundary conditions

$$\begin{aligned}
&\text{a)}\quad w = (1/\varepsilon)\xi_t + u\xi_x + v\xi_y \qquad ,\ z = -1 + \xi\\
&\text{b)}\quad w = \eta_t + \varepsilon u\eta_x + \varepsilon v\eta_y \qquad ,\ z = \varepsilon\eta\\
&\text{c)}\quad p = 0 \qquad ,\ z = \varepsilon\eta
\end{aligned} \tag{3}$$

Integrating the first equation 2.a) between the bed $-1+\xi$ and the free surface $\varepsilon\eta$, taking into account 3.a) and 3.b), yields the continuity equation (4):

$$\left[\eta - (1/\varepsilon)\xi\right]_t + \left[(1 - \xi + \varepsilon\eta)\bar{u}\right]_x + \left[(1 - \xi + \varepsilon\eta)\bar{v}\right]_y = 0 \tag{4}$$

where the bar over the variables represents the average value along the vertical. Then, accepting the fundamental hypothesis of the shallow water theory, $\sigma = h_0/\lambda << 1$, and developing the dependent variables in power series of the small parameter σ^2, that is

$$f = \sum_{i=0}^{\infty} (\sigma^2)^i f_i\ ,\ \text{for}\ f = (u, v, w, p, \eta, \xi, A) \tag{5}$$

where $A = u_x + v_y$, from continuity 2.a) and with 3.a) and 3.b) we obtain:

$$w_0 = -(z + 1 - \xi_0)A_0 + w_0^* \tag{6}$$
$$w_0^{**} = -(1 + \varepsilon\eta_0 - \xi_0)A_0 + w_0^* \tag{7}$$

where the simple and double asterisk represent the variables values at the bottom and at the surface, respectively. Of 2.e) we obtain, successively (Santos, 1989):

$$\begin{aligned}
u_0 &= u_0(x,y,t)\\
v_0 &= v_0(x,y,t)
\end{aligned} \tag{8}$$

$$\begin{aligned}
u_1 &= -(1/2)(z + 1 - \xi_0)^2 A_{0x}\\
&\quad + (z + 1 - \xi_0)(\xi_{0x}A_0 + w_{0x}^*) + u_1^*\\
v_1 &= -(1/2)(z + 1 - \xi_0)^2 A_{0y}\\
&\quad + (z + 1 - \xi_0)(\xi_{0y}A_0 + w_{0y}^*) + v_1^*
\end{aligned} \tag{9}$$

so that the average values of the horizontal components of the velocity, on the vertical, are given by:

$$\begin{aligned}
\bar{u} &= u_0 + \sigma^2 u_1^* - (\sigma^2/6)(1 + \varepsilon\eta_0 - \xi_0)^2 A_{0x}\\
&\quad + (\sigma^2/2)(1 + \varepsilon\eta_0 - \xi_0)(\xi_{0x}A_0 + w_{0x}^*) + O(\sigma^4)\\
\bar{v} &= v_0 + \sigma^2 v_1^* - (\sigma^2/6)(1 + \varepsilon\eta_0 - \xi_0)^2 A_{0y}\\
&\quad + (\sigma^2/2)(1 + \varepsilon\eta_0 - \xi_0)(\xi_{0y}A_0 + w_{0y}^*) + O(\sigma^4)
\end{aligned} \tag{10}$$

On the other hand, taking into account that,

$$f = f_0 + O(\sigma^2)\ \text{for}\ f = (u, v, \eta, \xi, w^*) \tag{11}$$

from (5) and (9) we obtain:

$$\begin{aligned}
u^{**} &= \bar{u} - (\sigma^2/3)(1 + \varepsilon\eta - \xi)^2 \bar{A}_x\\
&\quad + (\sigma^2/2)(1 + \varepsilon\eta - \xi)(\xi_x\bar{A} + w_x^*) + O(\sigma^4)\\
v^{**} &= \bar{v} - (\sigma^2/3)(1 + \varepsilon\eta - \xi)^2 \bar{A}_y\\
&\quad + (\sigma^2/2)(1 + \varepsilon\eta - \xi)(\xi_y\bar{A} + w_y^*) + O(\sigma^4)
\end{aligned} \tag{12}$$

Representing by $\Gamma = w_t + \varepsilon uw_x + \varepsilon vw_y + \varepsilon ww_z$ the vertical acceleration of the particles, we get $\Gamma = w_{0t} + \varepsilon u_0 w_{0x} + \varepsilon v_0 w_{0y} + \varepsilon w_0 w_{0z} + O(\sigma^2)$, and from (6), (7) and (11) the following approach is obtained:

$$\begin{aligned}
\Gamma &= -(z + 1 - \xi)(\bar{A}_t + \varepsilon\bar{u}\bar{A}_x + \varepsilon\bar{v}\bar{A}_y - \varepsilon\bar{A}^2)\\
&\quad + (w_t^* + \varepsilon\bar{u}w_x^* + \varepsilon\bar{v}w_y^*) + O(\sigma^2)
\end{aligned} \tag{13}$$

in which the terms within the two first parentheses represent the vertical acceleration when the bottom is horizontal, and the terms inside the third parenthesis represent the vertical acceleration along the real bottom. It should be noted that equation 2.d) can be written:

$$\varepsilon\sigma^2\Gamma = -p_z - 1 \tag{14}$$

where, for vertical integration between the bottom and the surface, the pressure p on the surface is obtained:

$$\begin{aligned}
p_x^{**} &= \varepsilon\eta_x(\varepsilon\sigma^2\Gamma^{**} + 1)\\
p_y^{**} &= \varepsilon\eta_y(\varepsilon\sigma^2\Gamma^{**} + 1)
\end{aligned} \tag{15}$$

which, along with 2b) and 2c), allow us to obtain (Santos, 1989):

$$\begin{aligned}&\left(u_t+\varepsilon uu_x+\varepsilon vu_y+\varepsilon wu_z\right)^{**}+\eta_x\left(1+\varepsilon\sigma^2\Gamma^{**}\right)=0\\&\left(v_t+\varepsilon uv_x+\varepsilon vv_y+\varepsilon wv_z\right)^{**}+\eta_y\left(1+\varepsilon\sigma^2\Gamma^{**}\right)=0\end{aligned}\tag{16}$$

or even, given that $\left(f_s\right)^{**}=f_s^{**}-\varepsilon\left(f_z\right)^{**}\eta_s$, where $f=(u,v)$ and $s=(x,y,t)$:

$$\begin{aligned}&u_t^{**}+\varepsilon u^{**}u_x^{**}+\varepsilon v^{**}u_y^{**}+\eta_x\left(1+\varepsilon\sigma^2\Gamma^{**}\right)=0\\&v_t^{**}+\varepsilon u^{**}v_x^{**}+\varepsilon v^{**}v_y^{**}+\eta_y\left(1+\varepsilon\sigma^2\Gamma^{**}\right)=0\end{aligned}\tag{17}$$

By developing expressions (17) in second approach (order 2 in σ^2), the following equations of motion (18) are obtained (Santos, 1989; Carmo, 2015):

$$\begin{aligned}&\overline{u}_t+\varepsilon\overline{u}\overline{u}_x+\varepsilon\overline{v}\overline{u}_y+\eta_x\\&\quad+\sigma^2\left\{\left[(2/3)(\varepsilon\eta-\xi)_x+(1/2)\xi_x\right]P+(1/3)(1+\varepsilon\eta-\xi)P_x\right\}\\&\quad+\sigma^2\left[\varepsilon\eta_xQ+(1/2)(1+\varepsilon\eta-\xi)Q_x\right]+O\left(\sigma^4\right)=0\\&\overline{v}_t+\varepsilon\overline{u}\overline{v}_x+\varepsilon\overline{v}\overline{v}_y+\eta_y\\&\quad+\sigma^2\left\{\left[(2/3)(\varepsilon\eta-\xi)_y+(1/2)\xi_y\right]P+(1/3)(1+\varepsilon\eta-\xi)P_y\right\}\\&\quad+\sigma^2\left[\varepsilon\eta_yQ+(1/2)(1+\varepsilon\eta-\xi)Q_y\right]+O\left(\sigma^4\right)=0\\&P=(1+\varepsilon\eta-\xi)\left(\varepsilon\overline{A}^2-\varepsilon\overline{u}\overline{A}_x-\varepsilon\overline{v}\overline{A}_y-\overline{A}_t\right)\\&Q=w_t+\varepsilon\overline{u}w_x+\varepsilon\overline{v}w_y\\&w=(1/\varepsilon)\xi_t+\overline{u}\xi_x+\overline{v}\xi_y\\&\overline{A}=\overline{u}_x+\overline{v}_y\end{aligned}\tag{18}$$

where, likewise, the bar over the variables represents the average value along the vertical. In dimensional variables and with a solid/fixed bottom ($\xi_t=0$), the complete set of equations is written, in second approach:

$$\begin{aligned}&h_t+\left(h\overline{u}\right)_x+\left(h\overline{v}\right)_y=0\\&\overline{u}_t+\overline{u}\overline{u}_x+\overline{v}\overline{u}_y+g\eta_x+\left[(2/3)h_x+(1/2)\xi_x\right]P\\&\quad+(1/3)hP_x+h_xQ+(1/2)hQ_x=0\\&\overline{v}_t+\overline{u}\overline{v}_x+\overline{v}\overline{v}_y+g\eta_y+\left[(2/3)h_y+(1/2)\xi_y\right]P\\&\quad+(1/3)hP_y+h_yQ+(1/2)hQ_y=0\\&P=h\left(\overline{A}^2-\overline{u}\overline{A}_x-\overline{v}\overline{A}_y-\overline{A}_t\right)\\&Q=w_t+\overline{u}w_x+\overline{v}w_y\\&w=\overline{u}\xi_x+\overline{v}\xi_y\\&\overline{A}=\overline{u}_x+\overline{v}_y\end{aligned}\tag{19}$$

where $h=h_0-\xi+\eta$ is total water depth. The one-dimensional form (1HD) of the equation system (19) is written, also with a fixed bottom:

$$\begin{aligned}&h_t+\left(\overline{u}h\right)_x=0\\&h\overline{u}_t+h\overline{u}\overline{u}_x+gh\eta_x\\&\quad+\left[h^2\left(P/3+Q/2\right)\right]_x+\xi_xh\left(P/2+Q\right)=0\\&P=-h\left(\overline{u}_{xt}+\overline{u}\overline{u}_{xx}-\overline{u}_x^2\right)\\&Q=\xi_x\left(\overline{u}_t+\overline{u}\overline{u}_x\right)+\xi_{xx}\overline{u}^2\end{aligned}\tag{20}$$

Assuming additionally a relative elevation of the surface due to the waves ($\varepsilon=a/h_0$) having a value close to the square of the relative depth ($\sigma=h_0/\lambda$), i.e. $O(\varepsilon)=O(\sigma^2)$, from the equation system (18), and at the same order of approximation, the following approach is obtained, in dimensional variables:

$$\begin{aligned}&h_t+\left(h\overline{u}\right)_x+\left(h\overline{v}\right)_y=0\\&\overline{u}_t+\overline{u}\overline{u}_x+\overline{v}\overline{u}_y+g\eta_x\\&\quad-(1/6)\xi_xP+(1/3)hP_x+(1/2)h_rQ_x=0\\&\overline{v}_t+\overline{u}\overline{v}_x+\overline{v}\overline{v}_y+g\eta_y\\&\quad-(1/6)\xi_yP+(1/3)h_rP_y+(1/2)h_rQ_y=0\end{aligned}\tag{21}$$

where $h_r=h_0-\xi$ is the water column height at rest, P and Q are given by $P=-\left(h_0-\xi\right)\left(\overline{u}_x+\overline{v}_y\right)_t$ and $Q=\left(\overline{u}\xi_x+\overline{v}\xi_y\right)_t$. The momentum equations are written:

$$\begin{aligned}&\overline{u}_t+\overline{u}\overline{u}_x+\overline{v}\overline{u}_y+g\eta_x+(1/6)h_r\xi_x\left(\overline{u}_x+\overline{v}_y\right)_t\\&\quad-(1/3)h_r^2\left(\overline{u}_x+\overline{v}_y\right)_{xt}+(1/3)h_r\xi_x\left(\overline{u}_x+\overline{v}_y\right)_t\\&\quad+(1/2)h_r\left(\overline{u}\xi_x+\overline{v}\xi_y\right)_{xt}=0\end{aligned}\tag{22}$$

$$\begin{aligned}&\overline{v}_t+\overline{u}\overline{v}_x+\overline{v}\overline{v}_y+g\eta_y+(1/6)h_r\xi_y\left(\overline{u}_x+\overline{v}_y\right)_t\\&\quad-(1/3)h_r^2\left(\overline{u}_x+\overline{v}_y\right)_{yt}+(1/3)h_r\xi_y\left(\overline{u}_x+\overline{v}_y\right)_t\\&\quad+(1/2)h_r\left(\overline{u}\xi_x+\overline{v}\xi_y\right)_{yt}=0\end{aligned}\tag{23}$$

with $\xi_t=0$, the complete system of equations (24) is obtained:

$$\begin{aligned}&h_t+\left(h\overline{u}\right)_x+\left(h\overline{v}\right)_y=0\\&\overline{u}_t+\overline{u}\overline{u}_x+\overline{v}\overline{u}_y+g\eta_x\\&\quad-(1/3)h_r^2\left(\overline{u}_{xxt}+\overline{v}_{xyt}\right)+h_r\xi_x\overline{u}_{xt}\\&\quad+(1/2)h_r\left(\xi_{xx}\overline{u}_t+\xi_y\overline{v}_{xt}+\xi_x\overline{v}_{yt}+\xi_{xy}\overline{v}_t\right)=0\\&\overline{v}_t+\overline{u}\overline{v}_x+\overline{v}\overline{v}_y+g\eta_y\\&\quad-(1/3)h_r^2\left(\overline{u}_{xyt}+\overline{v}_{yyt}\right)+h_r\xi_y\overline{v}_{yt}\\&\quad+(1/2)h_r\left(\xi_{yy}\overline{v}_t+\xi_y\overline{u}_{xt}+\xi_x\overline{u}_{yt}+\xi_{xy}\overline{u}_t\right)=0\end{aligned}\tag{24}$$

Further simplifying the equations of motion (18), retaining only terms up to order 1 in σ, i.e., neglecting all terms of dispersive origin, this system of equations is written in dimensional variables:

$$\begin{aligned} &h_t + (h\bar{u})_x + (h\bar{v})_y = 0 \\ &\bar{u}_t + \bar{u}\bar{u}_x + \bar{v}\bar{u}_y + g\eta_x = 0 \\ &\bar{v}_t + \bar{u}\bar{v}_x + \bar{v}\bar{v}_y + g\eta_y = 0 \end{aligned} \tag{25}$$

Approaches (19), (24) and (25) are known as Serre equations, or Green & Naghdi, Boussinesq and Saint-Venant, respectively, in two horizontal dimensions (2HD models). The classical Serre equations (19) (or Green & Naghdi, 1976) are fully-nonlinear and weakly dispersive. Boussinesq equations (24) only incorporate weak dispersion and weak non-linearity, and are valid only for long waves in shallow waters. As for the Boussinesq-type models, also Serre's equations are valid only for shallow water conditions.

3. Derivation and numerical formulation of higher order Serre equations

3.1. Mathematical derivation

To allow applications in a greater range of h_0/λ, other than shallow waters, a new set of extended Serre equations, with additional terms of dispersive origin, is developed and tested in Carmo (2013a,b) by comparisons with the available test data. The methodology used by Beji & Nadaoka (1996) and later by Liu & Sun (2005), to obtain an improved set of Boussinesq equations, was used to improve the dispersion characteristics of equations (20).

From the equation system (20), by adding and subtracting terms of dispersive origin, using the approximation $u_t = -g\eta_x$ and considering the parameters α, β and γ, with $\beta = 1.5\alpha - 0.5\gamma$, allows to obtain a new system of equations with improved linear dispersion characteristics:

$$\begin{aligned} &h_t + (uh)_x = 0 \\ &u_t + uu_x + g(h+\xi)_x + (1+\alpha)(\Omega u_t - hh_x u_{xt}) \\ &\quad - (1+\beta)\frac{h^2}{3}u_{xxt} + \alpha g\Omega(h+\xi)_x - \alpha g h h_x (h+\xi)_{xx} \\ &\quad - \beta g\frac{h^2}{3}(h+\xi)_{xxx} - hh_x uu_{xx} + \frac{h^2}{3}(u_x u_{xx} - uu_{xxx}) \\ &\quad + h(u_x)^2(h+\xi)_x + \xi_{xx}u^2(h+\xi)_x \\ &\quad + (\Omega + h\xi_{xx})uu_x + \frac{h}{2}\xi_{xxx}u^2 = 0 \end{aligned} \tag{26}$$

where $\Omega = \xi_x\eta_x + \frac{1}{2}h\xi_{xx} + (\xi_x)^2$.

After linearization of the equation system (26), the following dispersion relation is obtained, similar to the one obtained by Liu & Sun (2005) for an extended version of Boussinesq equations:

$$\frac{\omega^2}{gk} = \frac{kh_r\left[1 + (\alpha/2 - \gamma/6)(kh_r)^2\right]}{1 + \left[(1+\alpha)/2 - (1+\gamma)/6\right](kh_r)^2} \tag{27}$$

Comparing equation (27), written in terms of the phase speed (28)

$$C^2 = \frac{\omega^2}{k^2} = gh_r\left\{\frac{1 + (\alpha/2 - \gamma/6)(kh_r)^2}{1 + \left[(1+\alpha)/2 - (1+\gamma)/6\right](kh_r)^2}\right\} \tag{28}$$

with the linear dispersion relation $\omega^2/gk = tanh(kh_r)$, using the approach (29)

$$\begin{aligned} C_{Airy}^2 = \frac{\omega^2}{k^2} &= (gh_r)tanh(kh_r) \\ &= gh_r\left[\frac{1 + (1/15)(kh_r)^2}{1 + (2/5)(kh_r)^2}\right] + O\left[(kh)^6\right] \end{aligned} \tag{29}$$

allows to obtain values for the parameters α and γ. In a first approximation, we can suggest: $\alpha \approx 0.1308$ and $\gamma \approx -0.0076$ (Carmo, 2013a, b). It can be proven that a value of α within the interval $\alpha \in [0.13, 0.14]$ could be a good choice (Clamond *et al*., 2015). Considering these boundaries for α, the parameter γ will be within the interval $\gamma \in [-0.01, +0.02]$. It should be noted that with $\alpha \approx 2/15 = 0.1333$, as proposed by Madsen *et al*. (1991) and Madsen & Sørensen (1992) for an extended version of the Boussinesq equations, the value $\gamma = 0$ is obtained.

Different approaches for the wave and group celerity, up to order σ^4, can be found in Simarro (2013) and Simarro *et al*. (2015). Through analyses of the wave shoaling in one-layer, and comparing the shoaling errors for different sets of Boussinesq-type equations, Simarro (2013) propose the following values: $\beta = 0.06219$ instead of $\beta = 0.06667$, as also proposed by Madsen & Sorensen (1992), or $\beta = 0.15278$ instead of $\beta = 0.20$, as suggested by Beji & Nodaoka (1996). Using $\beta = 0.15278$ and with $\bar{\alpha} = 0.1350$, a value of $\gamma = -0.5117$ is obtained. It is thus evident that further studies on this matter are needed, but this is not the goal of the present work. Values of $\alpha \approx 0.1308$ and $\gamma \approx -0.0076$ are used in this work.

3.2. Numerical solution

The equation system (26) is solved using an efficient finite-difference method, whose consistency and stability are tested in Carmo (2013a,b) by comparison with a closed-form solitary wave solution of the Serre

equations. For this purpose, the terms containing derivatives in time of *u* are grouped. The final system of three equations is re-written according to the following equivalent form (SERIMP model) (Carmo, 2013a,b):

$$h_t + (uh)_x = 0 \tag{30a}$$

$$\begin{aligned} q_t &+ \left\{ uq - \frac{1}{2}\left[u^2 + (1+2\alpha) h^2 (u_x)^2 \right.\right. \\ &\left.\left. + (1+2\alpha)(\xi_x)^2 u^2 - h\,\xi_x (u^2)_x \right] \right\}_x \\ &+ \left[g(1+\alpha\Omega) + \alpha h\, u\, u_{xx} \right] \eta_x - \alpha g h h_x \eta_{xx} - \beta g \frac{h^2}{3} \eta_{xxx} \\ &- \frac{\alpha}{2}\left[(h\,\xi_{xx} u^2)_x + h_x \xi_{xx} u^2 - h\,\xi_{xx} u\, u_x \right] \\ &+ \left(\alpha - \frac{\beta}{3} \right) h^2 u_x u_{xx} + \beta \frac{h^2}{3} u\, u_{xxx} + \tau_b / (\rho h) = 0 \end{aligned} \tag{30b}$$

$$\left[1 + (1+\alpha)\Omega \right] u - (1+\alpha) h\, h_x u_x - (1+\beta) \frac{h^2}{3} u_{xx} = q \tag{30c}$$

$$\Omega = \xi_x \eta_x + \frac{1}{2} h\, \xi_{xx} + (\xi_x)^2 \tag{30d}$$

To compute the solution of equation system (30) (values of the variables *h* and *u* at time $t + \Delta t$) we use a numerical procedure based on the following scheme, itself based on the last equation system (30), for variables *h*, *q* and *u*. Knowing all values of h_i and u_i, $i = 1, N$, in the whole domain at time $n\Delta t$, the equations (30c) and (30d) are used to obtain the first values of q_i and Ω_i in the whole domain. Then, we continue with the following steps, in which the index *p* means predicted values (Carmo, 2013a,b):

(1) The first equation (30a) is used to predict the variable values h_{pi} at time $t + \Delta t$ ($h_{pi}^{t+\Delta t}$), in the whole domain.

(2) The second equation (30b) makes it possible to predict the variable values q_{pi} at time $t + \Delta t$ ($q_{pi}^{t+\Delta t}$), taking into account the values $\widetilde{h}_i^{t+\Delta t} = 0.5\left(h_i^t + h_{pi}^{t+\Delta t}\right)$, namely for Ω_i in the whole domain.

(3) The third equation (30c) makes it possible to compute the mean-averaged velocities $u_i^{t+\Delta t}$ at time $t + \Delta t$, taking into account the predicted values $h_{pi}^{t+\Delta t}$ and $q_{pi}^{t+\Delta t}$, namely for Ω_i in the whole domain.

(4) The first operation (step 1) is repeated in order to improve the accuracy of the variable values h_i at time $t + \Delta t$ ($h_i^{t+\Delta t}$), using the values $\overline{u}_i^{t+\Delta t} = 0.5\left(u_i^t + u_i^{t+\Delta t}\right)$ in the whole domain.

(5) Finally, the second operation (step 2) is repeated in order to improve the accuracy of the variable values q_i at time $t + \Delta t$ ($q_i^{t+\Delta t}$), taking into account the values $\overline{h}_i^{t+\Delta t} = 0.5\left(h_i^t + h_i^{t+\Delta t}\right)$ and $\overline{u}_i^{t+\Delta t} = 0.5\left(u_i^t + u_i^{t+\Delta t}\right)$ in the whole domain.

At each interior point *i*, the first, second and third-order spatial derivatives are approximated through centered differences and the time derivatives are approximated using forward differences. The convective terms $(uh)_x$ and $(uq)_x$ in equations (30a) and 30b) are approximated through centered schemes in space and time for variables *h* and *q*. At each time *t*, these terms are written in the following form:

$$\begin{aligned} (uh)_x &= u_i^t \left(\frac{h_{i+1}^t - h_{i-1}^t + h_{i+1}^{t+\Delta t} - h_{i-1}^{t+\Delta t}}{4\Delta x} \right) \\ &+ \frac{1}{2}\left(h_i^t + h_i^{t+\Delta t} \right) \left(\frac{u_{i+1}^t - u_{i-1}^t}{2\Delta x} \right) \end{aligned} \tag{31}$$

$$\begin{aligned} (uq)_x &= u_i^t \left(\frac{q_{i+1}^t - q_{i-1}^t + q_{i+1}^{t+\Delta t} - q_{i-1}^{t+\Delta t}}{4\Delta x} \right) \\ &+ \frac{1}{2}\left(q_i^t + q_i^{t+\Delta t} \right) \left(\frac{u_{i+1}^t - u_{i-1}^t}{2\Delta x} \right) \end{aligned} \tag{32}$$

All finite-difference equations are implicit. Therefore, the solution of system (30) requires, in each time step, the computation of five three-diagonal systems of N-2 equations (steps 1 to 5), which are easily computed using the three-diagonal matrix algorithm (TDMA), also known as the Thomas algorithm. The stability condition to be observed can be expressed in terms of the Courant/CFL number, and is given by:

$$C_R = \sqrt{gh}\,\frac{\Delta t}{\Delta x} < 1.0 \tag{33}$$

More accurate results are obtained with a domain discretization comprising about 25 to 30 points per wavelength and the condition (33) much lesser than unity, even below 0.5.

This numerical model (SERIMP) was used and tested in Carmo (2013a). With $\alpha = \beta = 0$, a comparison is presented with a closed-form solitary wave solution of these equations for a wave with $a/h0 = 0.60$. As can be seen, *the agreement between the numerical results and the analytical solution is perfect as much in wave amplitude as in phase* (Carmo, 2013a).

3.3. Boundary conditions

If an incident wave elevation $\eta(0,t)$ is given on the boundary (at $x = 0$) and the wave height is small compared to the water depth, the linear wave theory can be used to obtain the velocity of the incident wave

$$u(0,t)=\frac{\omega}{kh_r\left[1+(\beta/3)(kh_r)^2\right]}\eta(0,t) \quad (34)$$

where $\beta/3=\alpha/2-\gamma/6$ and $h_r=h_0-\xi$ is the water column height at rest on the boundary. Different kinds of wave patterns may be used. For mono-chromatic waves, the water-surface elevation $\eta(0,t)$ is given by $\eta(0,t)=a\sin(\omega t)$, where a, ω and k are, respectively, the wave amplitude, frequency and wave number.

In general, our goal at the output boundary is to avoid reflections of the wave. To do this, the domain is extended with a damping region of length L_{damp}. Terms like $-m(x)\eta$ and $-m(x)u$ may be added to the evolution equations for h and u, respectively. The length of the damped region is chosen such that we do not see any significant reflections. The implemented procedure is similar to that described in Zhang *et al*. (2014).

The terms $-m(x)\eta$ and $-m(x)u$ are added to the second member of *h*- and *u*-equations (26), respectively. As a first approximation, these terms can be written as:

$$-m(x)\eta=-\omega_1(x)\eta \quad (35)$$

$$-m(x)u=-\omega_1(x)u \quad (36)$$

where $\eta=h-h_0+\xi$ is the free surface elevation, $\omega_1(x)=(\tilde{\omega}_1/L_{damp})f(x)$, $\tilde{\omega}_1\approx 10\sqrt{gh}$, $L_{damp}\geq 10h$ is the sponge length, and

$$f(x)=\begin{cases}(n+1)(x/L_{damp})^n, & 0\leq x\leq L_{damp}\\ 0, & x<0\end{cases}, \quad n=2.$$

4. Applications of the 1HD extended Serre equations

4.1. Solitary wave travelling up a slope and reflection on a vertical wall

Experimental data and numerical results are available for a solitary wave propagating on the bathymetry shown in Figure 1 (Carmo, 2013a,b). It shows a constant depth before x = 55 m and a slope 1:50 between x = 55 m and x = 75 m. An impermeable vertical wall is placed at x = 75 m, corresponding to fully reflecting boundary conditions. A solitary wave of amplitude 0.12 m is initially centered at x = 25 m. The computational domain was uniformly discretized with a spatial step Δx = 0.05 m. A zero friction factor has been considered. Computations were carried out with a time step Δt = 0.010 s. Figure 2 compares numerical time series of surface elevation and test data at x = 72.75 m.

Figure 2 shows two peaks; the first one corresponding to the incident wave, and the second to the reflected wave. As pointed out in Carmo (2013a), the extended Serre model predictions for both peaks agree well with the measurements. *RMSE* values equal to 0.0090 m and 0.0117 m were found in first and second peaks, respectively, for the wave height. Regarding the phase, there is a loss of approximately 0.05 s and of 0.10 s in those peaks.

Predictions of the extended Boussinesq equations for both peaks are less accurate. Particularly for the reflected peak, this is overestimated in about 20%. This result is not surprising, given the lower validity of the Boussinesq model for waves of higher relative amplitude. Indeed, this model assumes $O(\varepsilon)\ll 1$, contrary to the Serre model, which is $O(\varepsilon)=1$. We used the extended Boussinesq model developed by Liu & Sun (2005). However, a similar study performed by Walkley & Berzins (1999), using the extended Boussinesq model developed by Nwogu (1993), shows no relevant differences in the graphs.

4.2. Periodic wave over an underwater bar

Beji & Battjes (1993) conducted experiments in a flume of 0.80 m wide with a submerged trapezoidal bar. The up- and down-wave bottom slopes of the submerged bar are 1:20 and 1:10 respectively. Before and after the bar, the water depth is 0.40 m, with a reduction to 0.10 m

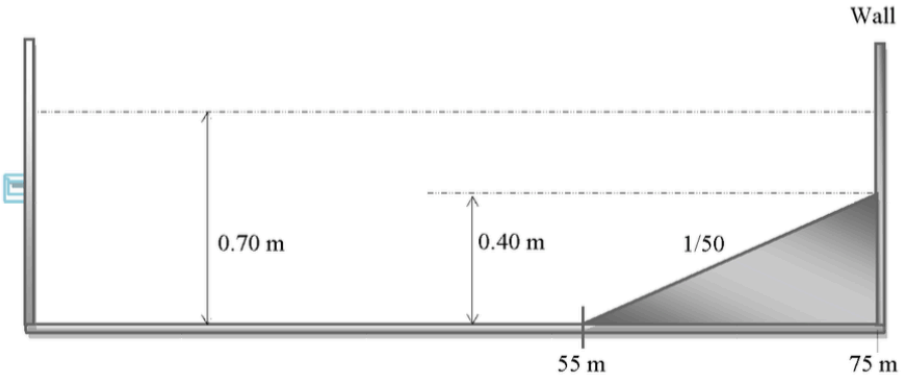

Figure 1 - Bathymetry for a solitary wave travelling up a slope and its reflection on a vertical wall (not in scale).

Figura 1 - Batimetria para a propagação de uma onda solitária sobre um trecho inclinado e sua reflexão numa parede vertical (fora de escala).

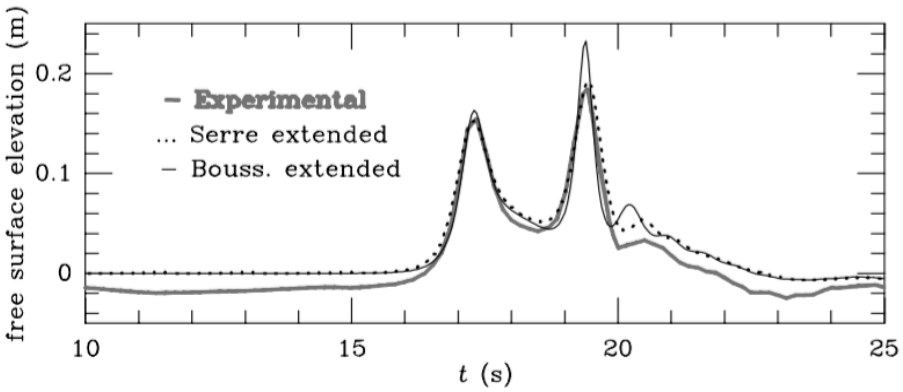

Figure 2 - Solitary wave travelling up a slope and its reflection on a vertical wall. Free surface elevation in a depth gauge located at x = 72.75 m. Experimental (———); Serre extended (·····); Boussinesq extended (——) (adapted from Carmo, 2013a).

Figura 2 - Propagação de uma onda solitária sobre um trecho inclinado e sua reflexão numa parede vertical. Variação da superfície livre numa sonda localizada em x = 72.75 m. Experimental (———); Serre com características dispersivas melhoradas (·····); Boussinesq com características dispersivas melhoradas (——) (adaptada de Carmo, 2013a).

above the bar, as shown in Figure 3. Experimental data obtained in this installation are available in the literature, and can be used for comparisons. The measured data are compared with numerical results of a 1HD extended version of the Boussinesq model (24), with $\alpha = 0.1308$ and $\gamma = -0.0076$, and the extended Serre equations (26) (SERIMP model) in Carmo (2013b), both improved with linear dispersive characteristics.

Comparisons are made in three wave gauges located at x = 10.5 m, x = 13.5 m and x = 17.3 m. For this purpose, a regular incident wave case with height 0.02 m, period T = 2.02 s and wavelength 3.73 m has been simulated. The computational domain was discretized with a uniform grid interval Δx = 0.025 m. A time step Δx = 0.0010s was used. Globally, numerical results of the improved Serre and Boussinesq models agree quite well with the measured data (Carmo 2013b).

Following is presented a comparison of the standard Serre's model (20) with the extended Serre equations (26) (SERIMP model). The standard Serre's model (20) is only valid for shallow waters, thus under conditions up to $h_0/\lambda = 0.05$. In this experiment, the dispersion parameter ($\sigma = h_0/\lambda$) is greater than 0.05 (about 0.11) in front and behind the bar, and therefore affects the validity of the numerical outcomes. Due to the fact that over the bar there are very shallow water conditions ($\sigma \approx 0.03$) the standard Serre equations are used considering the input boundary located at section x = 13.5 m, where the input signal is known (measured data). In this way, results of the Serre's standard model are not influenced, as would happen, by changes arising from the wave propagation before the bar, under intermediate water depths.

Figure 4 shows a comparison of numerical results of the standard Serre's model (20) with the extended Serre equations (26), considering, in the first case, the input boundary at x = 13.5 m (gauge signal) (Carmo, 2013b; 2015). The influence of additional terms of dispersive origin included in the extended Serre equations is clearly shown in Figure 4. The standard Serre model results (dashed line) are clearly of lesser quality. It should be noted that this application also demonstrates the good behavior of our numerical model to propagate a complex signal imposed at boundary.

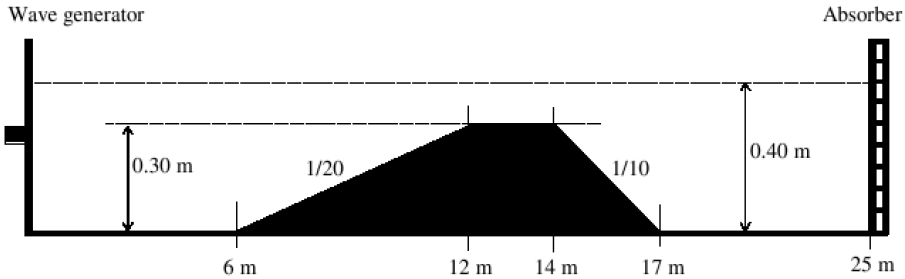

Figure 3 - Bathymetry for a periodic wave propagating over a bar (not in scale).

Figura 3 - Batimetria com barra sobre a qual se propaga uma onda periódica (fora de escala).

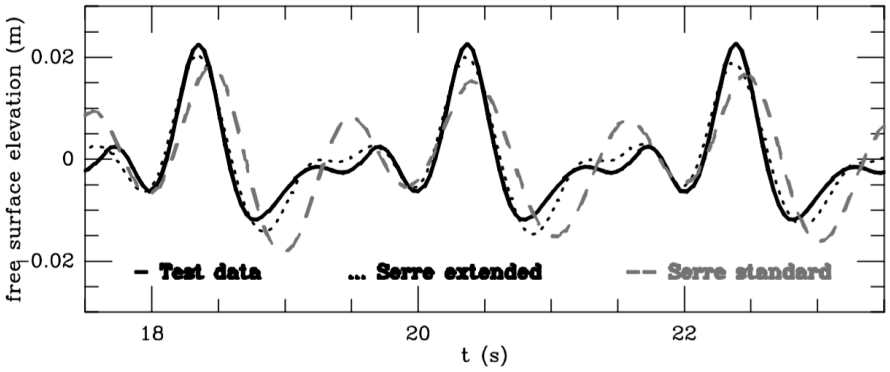

Figure 4 - Periodic wave propagating over a bar. Comparison of test data (——) with numerical results of the extended Serre model (26) (·····) and the standard Serre equations (20) (– – –) (adapted from Carmo, 2013b, 2015).

Figura 4 - Propagação de uma onda periódica sobre um fundo com barra. Comparação de dados experimentais (——) com resultados numéricos do modelo de Serre melhorado (26) (·····) e com resultados das equações clássicas de Serre (20) (– – –) (adaptada de Carmo, 2013b; 2015).

5. Sediment transport model

5.1. Mathematical formulation

The Bailard model (Bailard, 1981) does not consider the contribution of the wave acceleration-asymmetry in the sediment transport. As outlined in Dubarbier *et al.* (2015), models frequently used to estimate the evolution of beach profiles are inefficient with regard to the simulation of bottom shapes and migration of bars. This may be attributed to the absence of transport induced by acceleration-asymmetry of the wave.

In the following we use a 1HD model to compute the sediment transport in a channel, over a sand pit, and examine its ability to generate and propagate ripples and other bottom shapes. The morphodynamic model consists of the hydrodynamic equations (26) and the following sediment conservation equation (37) and a dynamic equation (38), in which four sediment transport processes are incorporated (Carmo, 2015):

$$(1-p)\xi_t + \langle q_{st} \rangle_x = 0 \tag{37}$$

$$\langle q_{st} \rangle = \langle q_{sl} \rangle + \langle q_{ss} \rangle + \langle q_{sk} \rangle + \langle q_{sy} \rangle \tag{38}$$

where

$$\langle q_{sl} \rangle = \frac{c_{sl}}{g(s-1)} \frac{\varepsilon_a}{tan\phi} \left(\langle |u|^2 u \rangle - \frac{1}{tan\phi} \xi_x \langle |u|^3 \rangle \right) \tag{39}$$

$$\langle q_{ss} \rangle = \frac{c_{ss}}{g(s-1)} \frac{\varepsilon_s}{w_s} \left(\langle |u|^3 u \rangle - \frac{\varepsilon_s}{w_s} \xi_x \langle |u|^5 \rangle \right) \tag{40}$$

$$\langle q_{sk} \rangle = c_{sk} \left(T_p U_{orb}^2 A_{sk} \right) \tag{41}$$

$$\langle q_{sy} \rangle = -c_{sy} \left(T_p U_{orb}^2 A_{asy} \right) \tag{42}$$

In equations (37) and (38), $\langle ... \rangle$ represents mean values of the arguments in the wave period, q_{st} is the net sediment transport, which is composed of the bedload transport, q_{sl}, the suspended load transport, q_{ss}, the *skewness* related transport, q_{sk}, and the transport related to wave asymmetry, q_{sy}; u is the wave velocity, p is the sediment porosity, ϕ is the internal angle of friction, $\varepsilon_a \in [0.10, 0.30]$ and $\varepsilon_s \in [0.01, 0.03]$ are efficiency coefficients, w_s is the sediment fall velocity, c_{sl} and c_{ss} are global rugosity coefficients, c_{sk} and c_{sy} are calibration coefficients. $U_{orb} = \pi H_{rms} / (T_p \sinh(kh))$ is the orbital velocity amplitude, $A_{sk} = \langle u^3 \rangle / \langle u^2 \rangle^{3/2}$ is a measure of orbital velocity-*skewness*, and $A_{asy} = \langle \{\mathbf{H}[u(t)]\}^3 \rangle / \langle u^2 \rangle^{3/2}$ is the velocity asymmetry coefficient, where $\mathbf{H}[u(t)]$ is the Hilbert transform of u. The asymmetry coefficient is here approximated by $A_{asy} = \langle a^3 \rangle / a_{rms}^3$, with $a_{rms} = \langle a^2 \rangle^{1/2}$, being a the wave acceleration.

All calibration coefficients, in particular the efficiencies (ε_a, ε_s) and (c_{sk}, c_{sy}), which represent the incomplete knowledge in our understanding of these processes, require a site-specific morphodyamic calibration. Once properly calibrated a comprehensive cross-shore profile model may predict the bar dynamics on the time-scale of days (at least). However, it must be noted that this calibration process is non-trivial since a large number of model coefficients is involved, typically requiring a large number of computations and optimization strategies. At a first approach, coefficients c_{sk} and c_{sy} are of the order of 10^{-6} to 10^{-5}, and are not necessarily equal. This work shows comparisons of numerical results considering $c_{sk} = c_{sy} = 5 \times 10^{-6}$ and $c_{sk} = c_{sy} = 10^{-5}$. Anyway, it should be noted that the effects are in a significant part determined by the calibration coefficient settings that have been kept constant.

Bed slope-related transport is included according to the Bailard equation increasing (decreasing) the down-slope

(up-slope) sediment transport. Equation (37) is easily computed using the Weighted Essentially Non-Oscillatory (WENO) scheme, as is presented in Long *et al*. (2008).

5.2. Numerical applications

Gardin (2004) compares the evolution of a bed profile with a pit using measurements and Delf3D computations. The sediment transport, especially cross-shore, was evaluated according to Bailard in the TRAN module of Delft3D software, which takes into account the effects of slope and wave asymmetry. According to the measurements, an important sedimentation offshore the pit is noted. Gardin (2004) concluded that the numerical model allows to obtain the pit evolution in agreement with the observations, with however a slight shift of the pit in the offshore direction.

The wave asymmetry effect is clearly shown in Groot (2005). Two transport formulas implemented in LOMOR model were applied in the prediction of the morphological behavior of a sandpit. The sediment transport due to wave asymmetry is neglected in both formulas. Numerical results of LOMOR using both formulas were compared with Delft3D computations. Delft3D takes into account velocity skewness and asymmetry. In all cases, the pit showed migration, damping and evolution of the slopes. However, contrary to LOMOR, Delft3D showed sedimentation downstream the pit.

Measured and modeled results of an offshore and onshore sandbar migration are shown in Zheng *et al*. (2014). The authors noted that the velocity skewness decreases from the seaward boundary toward the seaward flank of the initial bar, and then it increases over the initial bar and decreases over the area of final bar position, which is the region of active sandbar migration. After the final bar, velocity skewness increases toward the shoreline. The measured velocity asymmetry continuously increases from offshore and reaches its maximum shoreward of the final bar crest and then decreases toward the shoreline. Zheng *et al*. concluded that the onshore transport mainly appears where both velocity skewness and asymmetry are relatively high.

Based on 41 experiments, Berni *et al*. (2012) obtained a large range of values for the free-stream skewness and large values of the asymmetry. The authors analyzed numerically and experimentally the asymmetry transformation process to skewness within the boundary layer. They concluded that this transformation results in skewed velocities near the bed that lead directly to net sediment transport.

The dominant hydrodynamic processes governing cross-shore sandbar behavior have been discriminated by Dubarbier *et al*. (2015) using four modes of sediment transport driven by wave skewness and asymmetry, mean current and slope effects. They concluded that acceleration–skewness-induced transport systematically results in a slow onshore sandbar migration together with a slow bar growth. They also concluded that velocity–skewness-induced transport can drive onshore and offshore bar migrations with substantially larger rates.

A morphodynamic model (MORSYS) was used by Rosa *et al*. (2011) to study the evolution of a sand pit offshore Vale do Lobo (Algarve, Portugal). The authors conclude that the simulations performed for a whole period of 2.5 years and during one month encompassing two storm events show similar trends for the morphological evolution of the sandpit. The obtained results allowed to evaluate the good performance of the numerical model.

Sand extractions and formation of sand pits is a common activity in coastal zones. Therefore, the sand pit evolution, and in particular its migration and rate of replenishment should be reproduced with sufficient accuracy. Following, the evolution of a sand pit is studied using the morphodynamic model described above.

In our numerical experiment, a wave with the following characteristics is considered: height H = 0.20 m, period T = 8 s, and wavelength λ = 24.8 m. This wave is introduced at the upstream boundary and propagated along a horizontal channel 1.0 m depth in the first 28.75 m. From this point there is a sand pit, with the upstream face having a slope 9.82% down to a minimum $\xi = -0.275$ and left constant between 31.55 m and 32.175 m. Then the pit increases up to $\xi = 0$, having this face a positive slope 18.64%. A median diameter $d_{50} = 1.0$ mm is representative of the bottom grain size.

Figure 5 shows the simulated wave along the channel with a sand pit, between 15 m and 45 m. The wave transformations that occurred are evident, increasing the *skewness* and asymmetry of the wave. Figure 6 shows bottom configurations obtained 450 waves after, corresponding to a simulation time of 60 minutes, considering the first two terms $\mathbf{q}_{sl}$, and $\mathbf{q}_{ss}$ of equation (38) (dashed line) and all terms of this equation with $c_{sk} = c_{sy} = 5\text{x}10^{-6}$ (dotted line). Figure 7 shows bottom configurations obtained 450 waves after, corresponding to a simulation time of 60 minutes, considering all terms of equation (38) with $c_{sk} = c_{sy} = 5\text{x}10^{-6}$ (dotted line) and with $c_{sk} = c_{sy} = 10^{-5}$ (bold line), respectively.

Although lacking experimental evidence, the presented results seem to translate the physical phenomena. Indeed, they exhibit identical behavior to that shown in the measured and simulated examples in the literature above. Observing Figures 6 and 7, a preliminary conclusion can be drawn. Excluding the transport associ-

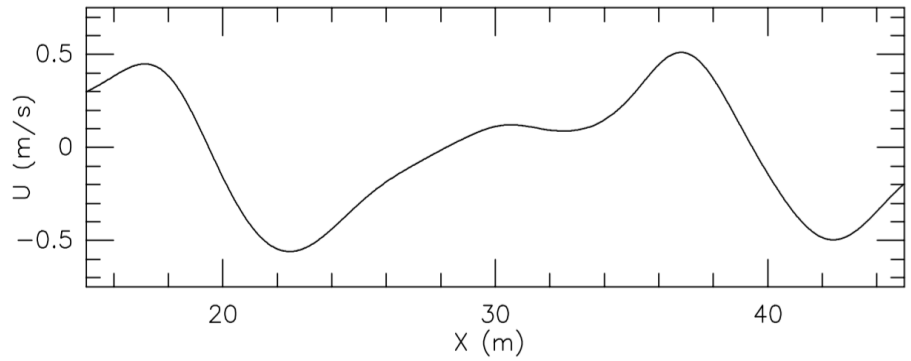

Figure 5 - Initial velocity of the wave propagating over a sandpit.

Figura 5 - Velocidade inicial da propagação de uma onda sobre uma cova de areia.

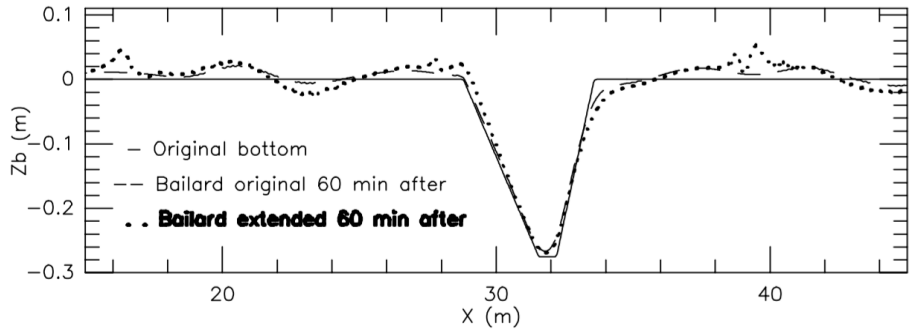

Figure 6 - Bottom profiles after 60 minutes of simulation, considering terms $\mathbf{q}_{sl}$ and $\mathbf{q}_{ss}$ of equation (38) (dashed line), and all terms $\mathbf{q}_{sl}$, $\mathbf{q}_{ss}$, $\mathbf{q}_{sk}$ and $\mathbf{q}_{sy}$ of this equation with $c_{sk} = c_{sy} = 5\text{x}10^{-6}$ (dotted line).

Figura 6 - Configurações do fundo após 60 minutos de simulação, considerando os termos $\mathbf{q}_{sl}$ e $\mathbf{q}_{ss}$ da equação (38) (linha tracejada), e todos os termos $\mathbf{q}_{sl}$, $\mathbf{q}_{ss}$, $\mathbf{q}_{sk}$ e $\mathbf{q}_{sy}$ desta equação com $c_{sk} = c_{sy} = 5\text{x}10^{-6}$ (linha ponteada).

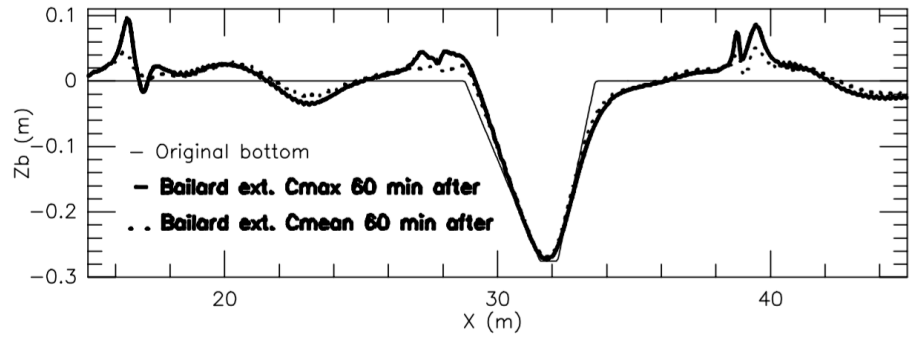

Figure 7 - Bottom profiles after 60 minutes of simulation, considering all terms $\mathbf{q}_{sl}$, $\mathbf{q}_{ss}$, $\mathbf{q}_{sk}$ and $\mathbf{q}_{sy}$ of equation (38) with $c_{sk} = c_{sy} = 5\text{x}10^{-6}$ (dotted line) and with $c_{sk} = c_{sy} = 10^{-5}$ (bold line).

Figura 7 - Configurações do fundo após 60 minutos de simulação, considerando os termos $\mathbf{q}_{sl}$, $\mathbf{q}_{ss}$, $\mathbf{q}_{sk}$ e $\mathbf{q}_{sy}$ da equação (38) com $c_{sk} = c_{sy} = 5\text{x}10^{-6}$ (linha ponteada) e com $c_{sk} = c_{sy} = 10^{-5}$ (linha carregada).

ated with the wave velocity-*skewness* and the acceleration-asymmetry reduces the onshore sediment transport (in the wave direction). Another evidence is the large difference in the bottom configurations considering relatively close values of c_{sk} and c_{sy}, thus showing great sensitivity to small variations of the involved constants.

6. Conclusions

Analytical developments and results of the numerical models presented in this work are promising enough to warrant further developments in both fields of the hydrodynamics and morphodynamics.

In hydrodynamic terms, extended versions of Boussinesq type models have shown a good performance. Less common are models of extended Serre equations, example of which is the model translated by equations (26); however, as is widely recognized, under certain conditions, the Serre equations more accurately simulate the behavior of the physical phenomena than Boussinesq type models.

In morphodynamic terms, it is known that the term $<|\boldsymbol{u}^2|\boldsymbol{u}>$ is associated with the short wave asymmetry and *skewness* in the surf zone. It is zero when there is no short wave *skewness* and a positively skewed wave results in an onshore directed transport. Consequently, as is reported in literature and this work also shows, the wave asymmetric oscillatory flow contributes to a shoreward directed net sediment transport.

The numerical results presented in this work, although qualitative, seem to translate the physical behavior of the processes involved. It is clearly shown that the *skewness* and wave asymmetry lead to an increase of the sediment transport in the wave direction.

An extended version of the two-dimensional equation system (19) with improved linear dispersion characteristics and using a finite element method is being developed and will be published soon. Also the experimental validation of the morphodynamic model will take place as quickly as possible.

Appendix

Supporting Information associated with this article is available online at **http://www.aprh.pt/rgci/pdf/rgci-660_Carmo_Supporting-Information.pdf**

References

Bailard, J.A. (1981) - An energetics total load sediment transport model for a plane sloping beach. *Journal of Geophysical Research*, 86(C11):10938-10954. DOI: 10.1029/JC086iC11p10938.

Beji, S.; Battjes, J.A. (1993) - Experimental investigations of wave propagation over a bar. *Coastal Engineering,* 19(1-2):151-162. DOI: 10.1016/0378-3839(93)90022-Z.

Beji, S.; Nadaoka, K., 1996. A formal derivation and numerical modelling of the improved Boussinesq equations for varying depth, *Ocean Engineering*, 23(8):691. DOI: 10.1016/0029-8018(96)84408-8.

Berkhoff, J.C.W.; Booij, N.; Radder, A.C. (1982) - Verification of numerical wave propagation models foe simple harmonic linear water waves. *Coastal Engineering,* 6:255-279. DOI: 10.1016/0378-3839(82)90022-9.

Berni, C.; Suarez, L.; Michallet, M.; Barthélemy, E. (2012) – Asymmetry and skewness in the bottom boundary layer: Small scale experiments and numerical model. 33rd International Conference on Coastal Engineering (25), Santander, Spain. Available online at https://icce-ojs-tamu.tdl.org/icce/index.php/icce/article/view/6637.

Booij, N. (1983) - A note on accuracy of the mild-slope equation. *Coastal Engineering*, 7(3):191-203. DOI: 10.1016/0378-3839(83)90017-0.

Boussinesq, J. (1872) - Théorie des ondes et des remous qui se propagent le long d'un canal rectangulaire horizontal. *Journal of Mathématiques Pures et Appliquées*, 2(17):55-108. Available online at https://eudml.org/doc/234248

Carmo, J.S. Antunes do ; Seabra-Santos, F.J. (1996) - On breaking waves and wave-current interaction in shallow water: A 2DH finite element model. *International Journal for Numerical Methods in Fluids,* 22:429-444. DOI: 10.1002/(SICI)1097-0363(19960315)22:5<429::AID-FLD388>3.0.CO;2-8

Carmo, J.S. Antunes do (2013a) - Boussinesq and Serre type models with improved linear dispersion characteristics: Applications. *Journal of Hydraulic Research*, IAHR, 51(6):719-727. DOI: 10.1080/00221686.2013.814090.

Carmo, J.S. Antunes do (2013b) - Extended Serre Equations for Applications in Intermediate Water Depths. *The Open Ocean Engineering Journal*, 6:16-25. DOI: 10.2174/1874835X01306010016.

Carmo, J.S. Antunes do (2015) - Sediment transport induced by *skewness* and asymmetry of the wave. In (*book*) *VIII Symposio sobre el Margen Continental Ibérico Atlántico*, 121-124, V. Díaz del Río, P.Bárcenas, L.M. Fernández-Salas, N. López-González, D. Palomino, J.L.Rueda, O.Sánchez-Guillamón e J.T.Vásquez (Editors). Ediciones Sia Graf, Málaga, Spain. Available online at https://www.researchgate.net/publication/282009789_Sediment_transport_induced_by_skewness_and_asymmetry_of_the_wave

Clamond, D.; Dutykh, D.; Mitsotakis, D. (2015) - *Conservative modified Serre-Green-Naghdi equations with improved dispersion characteristics*, 22 pages. Available online at http://arxiv.org/pdf/1511.07395.pdf

Dalrymple, R.A. (1988) - Model for refraction of water waves. *Journal of Waterway, Port, Coastal, and Ocean Engineering*, ASCE, 114(4):423-435. DOI: 10.1061/(ASCE)0733-950X(1988)114:4(423).

Dubarbier, B.; Castelle, B.; Marieu, V.; Ruessink, G. (2015) - Process-based modeling of cross-shore sandbar behavior. *Coastal Engineering*, 95:35–50. DOI: 10.1016/j.coastaleng.2014.09.004.

Gardin, B. (2004) - Numerical simulation of the impact of a sandpit on the shore stability, following Migniot and Viguier's experiments (1979). *VIIIèmes Journées Nationales Génie Côtier - Génie Civil*, Compiègne, France. Available online at http://wwz.ifremer.fr/gm_eng/content/download/18041/264573/file/dugardin_GCGC2004_uk.pdf

Green, A.E.; Naghdi, P.M. (1976) - A derivation of equations for wave propagation in water of variable depth. *Journal of Fluid Mechanics*, 78(2), 237-246. DOI: 10.1017/S0022112076002425.

Groot, P.J. (2005) - Modelling the morphological behaviour of sandpits. Influence sediment transport formula and verification of a 1DH model. Report carried out in the framework of the European project SANDPIT, University of Twente, The Netherlands. Available online at https://www.utwente.nl/ctw/wem/education/afstuderen/afstudeerverslagen/2005/de groot.pdf

Kirby, J.T. (1984) - A note on linear surface wave-current interaction over slowly varying topography. *Journal of Geophysical Research*, 89©:745-747. DOI: 10.1029/JC089iC01p00745.

Kirby, J.T.; Dalrymple, R.A. (1983) - A parabolic equation for the combined refraction-diffraction of stokes waves by mildly varying topography. *Journal of Fluid Mechanics*, 136:435-466. DOI: 10.1017/S0022112083002232.

Liu, Z.B.; Sun Z.C. (2005) - Two sets of higher-order Boussinesq-type equations for water waves. *Ocean Engineering* 32(11-12):1296-1310. DOI: 10.1016/j.oceaneng.2004.12.004.

Long, W.; Kirby, J.T.; Shao, Z. (2008) - A numerical scheme for morphological bed level calculations. *Coastal Engineering*, 55(2):167–180. DOI: 10.1016/j.coastaleng.2007.09.009.

Madsen, P.A.; Murray, R.; Sørensen, O.R. (1991) - A new form of the Boussinesq equations with improved linear dispersion characteristics. *Coastal Engineering*, 15(4):371-388. DOI: 10.1016/0378-3839(91)90017-B.

Madsen, P.A.; Sørensen, O.R. (1992) - A new form of the Boussinesq equations with improved linear dispersion

characteristics. Part 2. A slowly-varying bathymetry. *Coastal Engineering*, 18(3-4):183–204. DOI: 10.1016/0378-3839(92)90019-Q.

Nwogu, O. (1993) - Alternative form of Boussinesq equations for nearshore wave propagation. *Journal of Waterway, Port, Coastal, and Ocean Engineering*, 119(6):618-638. DOI: 10.1062/(ASCE)0733-950X(1993)119.6(618).

Rosa, J.; Gonçalves, D.; Silva, P.A.; Pinheiro, L.M.; Rebêlo, L.; Fortunato, A.; Bertin, X. (2011) - Sand Extraction Evolution Area offshore Vale do Lobo (Algarve, Portugal) - comparison between numerical results and bathymetric data. *Journal of Integrated Coastal Zone Management*, 11(3):369-377. DOI: 10.5894/rgci284.

Santos, F.J. Seabra (1985) - *Contribution a l'ètude des ondes de gravité bidimensionnelles en eau peu profonde*. Ph.D. thesis, Université Scientifique et Médicale et Institut National Polytechnique de Grenoble, France (*in French*). *Unpublished*.

Santos, F.J. Seabra (1989) - As aproximações de Wu e de Green & Naghdi no quadro geral da teoria da água pouco profunda. *Simpósio Luso-Brasileiro de Hidráulica e Recursos Hídricos* (4º SILUSBA), Lisboa, Portugal, 14-16 June, 209-219 (*in Portuguese*). *Unpublished*.

Serre, F. (1953) - Contribution à l'étude des écoulements permanents et variables dans les canaux. *La Houille Blanche*, 8(6):374–388. DOI: http://dx.doi.org/10.1051/lhb/1953058.

Simarro, G. (2013) - Energy balance, wave shoaling and group celerity in Boussinesq-type wave propagation models. *Ocean Modelling*, 72:74-79. DOI: 10.1016/j.ocemod.2013.08.004.

Simarro, G.; Orfila, A.; Mozos, C.M.; Pruneda, R.E. (2015) - On the linear stability of one- and two-layer Boussinesq-type equations for wave propagation over uneven beds. *Ocean Engineering*, 106:446-457. DOI: 10.1016/j.oceaneng.2015.07.022.

Walkley, M.A.; Berzins, M. (1999) - A finite element method for the one-dimensional extended Boussinesq equations. *International Journal for Numerical Methods in Fluids*, 29(2):143-157. DOI: 10.1002/fld.349.

Zhang Y.; Kennedy, A.B.; Panda, N.; Dawson, C.; Westerink, J.J. (2014) – Generating-absorbing sponge layers for phase-resolving wave models. *Coastal Engineering*, 84:1–9. DOI: 10.1016/j.coastaleng.2013.10.019.

Zheng, J.; Zhang, C.; Demirbilek, Z.; Lin, L. (2014) – Numerical study of sandbar migration under wave-undertow interaction. *Journal of Waterway, Port, Coastal, and Ocean Engineering*, 140(2):146-159. DOI: 10.1061/(ASCE)ww.1943-5460.0000231.